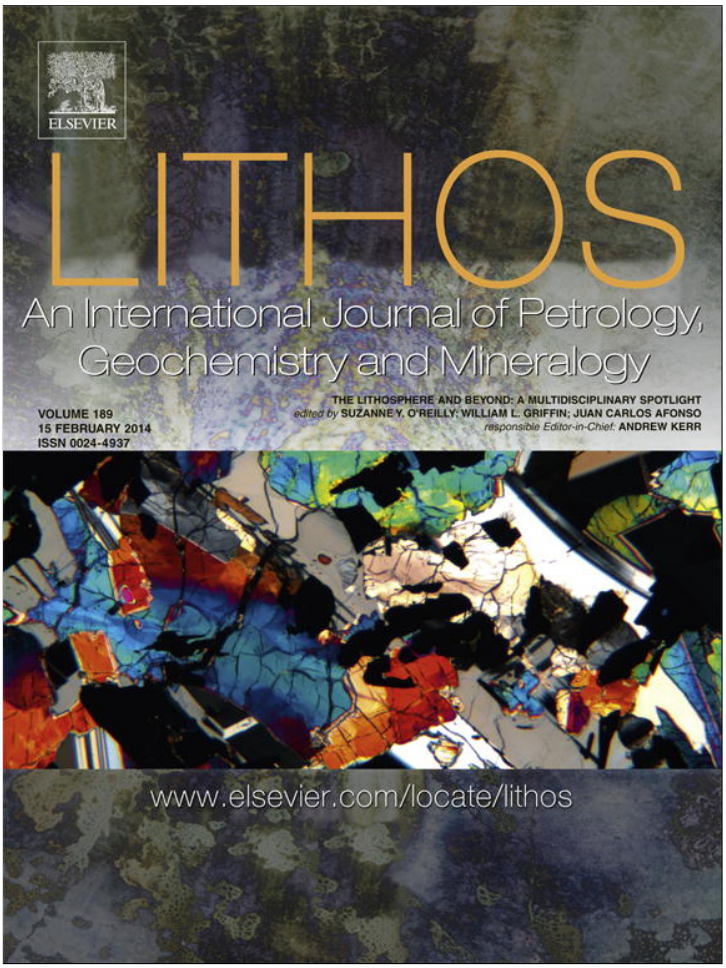

Lithos 189 (2014) 16–27

Contents lists available at ScienceDirect

Lithos

journal homepage: www.elsevier.com/locate/lithos

Coupled mantle dripping and lateral dragging controlling the lithosphere structure of the NW-Moroccan margin and the Atlas Mountains: A numerical experiment

Sergio Zlotnik [a,*], Ivone Jiménez-Munt [b], Manel Fernàndez [b]

[a] Laboratori de Calcul Numeric, Dep. de Matematica Aplicada III, Universitat Politecnica de Catalunya Campus Nord UPC, Barcelona, Spain
[b] Group of Dynamics of the Lithosphere, Institute of Earth Science Jaume Almera, CSIC, Barcelona, Spain

ARTICLE INFO

Article history:
Received 11 May 2013
Accepted 21 October 2013
Available online 30 October 2013

Keywords:
Moroccan margin
Continental passive margin
Atlas Mountains
Lithospheric structure
Numerical modelling

ABSTRACT

Recent studies integrating gravity, geoid, surface heat flow, elevation and seismic data indicate a prominent lithospheric mantle thickening beneath the NW-Moroccan margin (LAB >200 km-depth) followed by thinning beneath the Atlas Domain (LAB about 80 km-depth). Such unusual configuration has been explained by the combination of mantle underthrusting due to oblique Africa–Eurasia convergence together with viscous dripping fed by asymmetric lateral mantle dragging, requiring a strong crust–mantle decoupling. In the present work we examine the physical conditions under which the proposed asymmetric mantle drip and drag mechanism can reproduce this lithospheric configuration. We also analyse the influence of varying the kinematic boundary conditions as well as the mantle viscosity and the initial lithosphere geometry. Results indicate that the proposed drip–drag mechanism is dynamically feasible and only requires a lateral variation of the lithospheric strength. The further evolution of the gravitational instability can become either in convective removal of the lithospheric mantle, mantle delamination, or subduction initiation. The model reproduces the main trends of the present-day lithospheric geometry across the NW-Moroccan margin and the Atlas Mountains, the characteristic time of the observed vertical movements, the amplitude and rates of uplift in the Atlas Mountains and offers an explanation to the Miocene to Pliocene volcanism. An abnormal constant tectonic subsidence rate in the margin is predicted.

1. Introduction

Passive margins are characterized by a progressive seaward thinning of the continental crust which eventually breaks up and becomes a transitional-to-oceanic crust type. The crustal thickness commonly varies from 30–40 km in the stable continental region to 6–8 km in the deep oceanic domain (excluding sea-water layer). Variations in the total lithospheric thickness or in the depth of the lithosphere–asthenosphere boundary (LAB) depend on the age of both the continental and the oceanic domains.

The LAB depth in the oceanic domain varies with age for $t \leq 70$ My (e.g., Turcotte and Oxburgh, 1967; Turcotte and Schubert, 1982) resulting in values of 60–65 km for lithospheres ~25 My old and 105 km for ages of 70 My. Older lithospheres respond better to the plate-cooling model (e.g., Parsons and Sclater, 1977; Stein and Stein, 1992) where the LAB depth reaches values of 120–130 km for lithospheres older than 120 My.

In the stable continental domain the LAB depth can vary from 100–140 km in Phanerozoic areas, to 150–180 km in Proterozoic regions, and to >250 km in Archean areas (Artemieva, 2006; Artemieva, 2011; Poudjom Djomani et al., 2001). Therefore, depending on the age of the rifted continental domain and the time since rifting occurred, the LAB depth across a passive continental margin can be nearly constant as occurs in the Iberian–Atlantic margin (e.g., Fernandez et al., 2004a; Torne et al., 1995), or strongly decreasing seawards as occurs in the Norwegian margin (Fernandez et al., 2004b, 2005) or in the Namibia margin (Fernández et al., 2010).

Contrarily to the common mode of deformation described above, recent studies integrating gravity, geoid, surface heat flow, elevation and seismic data indicate prominent atypical variations of the LAB geometry across the NW-Moroccan margin and the Atlas Mountains. Previous works propose a lithospheric structure where the LAB lies at 110–120 km depth beneath the deep oceanic domain and dips to approximately 140 km under the continental margin (Fullea et al., 2007, 2010; Missenard et al., 2006; Teixell et al., 2005; Zeyen et al., 2005). Jiménez-Munt et al. (2011), however, propose that the LAB under the margin reaches 200 km in thickness. Further to the SE, the lithospheric mantle thins by more than 130 km and the LAB shallows to ~80 km depth beneath the Atlas Mountains and dips again towards the West African Craton reaching values of ~170 km depth.

The large variations in the lithospheric mantle thickness contrast with the more homogeneous crustal structure. Main variations in

* Corresponding author.
E-mail address: sergio.zlotnik@upc.edu (S. Zlotnik).

0024-4937/$ – see front matter © 2013 Elsevier B.V. All rights reserved.
http://dx.doi.org/10.1016/j.lithos.2013.10.016

crustal thickness are related to the rifted passive margin with Moho depths varying from 34 km in the stable Moroccan Plateau to 15 km in the oceanic domain, and in the intracontinental fold belt of the Atlas Mountains where recent seismic data show maximum crustal thickness values of ~40 km (Fullea et al., 2007, 2010; Missenard et al., 2006; Teixell et al., 2005). These differences in the crust and lithosphere mantle geometries evidence that the NW-Moroccan margin is dominated by a strong crust-mantle strain. Decoupling between crust and mantle is also evidenced by the contrasting widths of the regions over which crust and mantle shortening are accommodated as well as the respective amounts of shortening. Whereas crustal shortening, estimated in 40–60 km, is accommodated sparsely over a ~950 km wide region, most of the lithospheric mantle shortening, which could amount ~150 km, is absorbed on the Moroccan margin over a ~400 km wide region. To solve this shortening paradox, Jiménez-Munt et al. (2011) propose a model in which mantle underthrusting beneath the margin accommodates 50–60 km of convergence and triggers mantle dripping and lateral dragging of the mantle material missing beneath the Atlas.

Previous studies have shown that Rayleigh–Taylor gravitational instabilities may play a fundamental role in the tectonics of continental orogens, particularly in explaining the crust — mantle strain partitioning and coupled lithospheric mantle thinning and thickening (e.g., Göğüş and Pysklywec, 2008; Harig et al., 2010; Houseman and Gemmer, 2007; Houseman et al., 1981, 2000; Marotta et al., 1998, 1999; Molnar and Houseman, 2004; Valera et al., 2011). The resulting lithospheric deformation geometries depend on the rate of imposed convergence and on the relative strengths and buoyancies of crust and mantle lithosphere (Houseman et al., 2000). A moderate shortening, <10% for dry olivine and 1% for wet olivine, suffices to generate mantle instability (Houseman and Molnar, 2001). For a low viscosity ratio between crust and lithosphere or a buoyant crust, downwelling flow develops on the flanks of the zone of convergence, and dramatic lithospheric thinning occurs beneath the centre of the convergent zone resembling a delamination process as conceived by (Bird, 1978). Convective removal with asymmetric mantle drip and dragging has been proposed to explain the geodynamic evolution of the Tyrrhenian and Alboran basins in Western Mediterranean, Tien Shan and Tibetan Plateau in Central Asia (Houseman and Molnar, 2001, 2004) and the Southeastern Carpathians (Gemmer and Houseman, 2007; Lorinczi and Houseman, 2009).

Several mechanisms have been proposed to explain the evolution of the Atlas Mountains and particularly to relate the presence of a relatively thin lithospheric mantle to high uplift rates and alkaline volcanism since Eocene to Quaternary. These mechanisms include mantle upwelling related to “baby plume” like structures (e.g., Babault et al., 2008; Missenard et al., 2006; Teixell et al., 2005; Zeyen et al., 2005), mantle delamination related to slab roll-back in the Western Mediterranean (Duggen et al., 2009), small-scale or edge-driven convection related to sharp lateral lithospheric thickness variations (e.g., Fullea et al., 2010; Missenard and Cadoux, 2012), and coupled drip–drag mechanism (Jiménez-Munt et al., 2011). The latter work relates the lithospheric thinning affecting the Atlas Mountains to the lithospheric thickening affecting the NW-Moroccan margin.

In this work we present a fully dynamic numerical experiment with the aim to examine under which conditions the proposed asymmetric mantle drip and drag mechanism can reproduce lithospheric mantle thickening beneath a passive continental margin and mantle thinning beneath an adjacent intracontinental orogen. The numerical approach uses the Underworld package (Moresi et al., 2003) with a modelling domain that extends down to 670 km depth and allows for introducing tectonic convergence and spatial variations of key parameters (viscosity, density, heat production, etc.) for the different layers. A key aspect of the study is its application to the NW-Moroccan margin and Atlas Mountains by reproducing the main features of the present-day lithospheric geometry, the characteristic time of the process and the associated vertical movements.

2. Numerical method and model setup

The geodynamic process is modelled as a visco-plastic flow in a two-dimensional Cartesian geometry. The governing momentum, mass and energy conservation equations are solved via the Underworld modelling framework (Moresi et al., 2003). As usual in mantle modelling, the momentum conservation takes the form of the Stokes equation, as the inertial and convective terms are neglected (Schubert et al., 2001). Conservation of energy is solved considering viscous heating, adiabatic heating and a heat source term due to radiogenic elements.

The initial setup of the model, shown in Fig. 2, corresponds to a 60 Ma version of the structure of the Moroccan margin proposed by Jiménez-Munt et al. (2011). It represents a ~2000 km long and 660 km deep transect corresponding, approximately, to a line from the Gorringe Bank to the West African Craton. Therefore, this transect crosses four different lithospheric domains (Figs. 1 and 2): i) a mature oceanic lithosphere at the northwest, ii) a passive continental margin, iii) a continental lithosphere with the Atlas Mountains range and, finally iv) the West African Craton.

These four domains are included in the numerical experiment and have distinct characteristics. The oceanic domain is composed by a 110 km thick lithosphere with an 8 km thick oceanic crust. Marine sediments are not included in the model. The rheology of the oceanic lithosphere plays an important role in the dynamics of the models and deserves some attention. The oceanic lithosphere is not only a thermal, but also a chemical and a mechanical boundary layer. Its thermodynamic properties, which in turn control its dynamic behaviour, depend ultimately on temperature, pressure, composition of the original source (i.e., upper mantle that has not experienced partial melting), and degree of melt depletion experienced at the MOR (Afonso et al., 2007, 2008; Hirth and Kohlstedt, 1996; Lee et al., 2005; Phipps Morgan, 1997; Zlotnik et al., 2008). Pressure-release melting at mid-ocean ridges generates compositional and rheological layering in the oceanic mantle. Several recent numerical and theoretical studies of subduction dynamics introduced a high viscosity layer (so-called *strong core*) in the rheology of the oceanic mantle, e.g., (Capitanio et al., 2011; Ribe, 2010; Ribe et al., 2007; Schellart et al., 2011; Stegman et al., 2010). We adopt the same kind of rheological stratification for the oceanic domain. This particular layering is not expected in the continental domain so in the passive margin the strong core is transitionally reduced.

The second domain represents the passive continental margin. The initial lithospheric thickness increases from 110 to 140 km and a transitional crust thickens gradually towards the continent until converted in an upper and lower continental crust with thicknesses of 23 and 12 km respectively, coinciding with the estimations by Contrucci et al. (2004).

The third continental domain includes the Atlas Mountains range. Beneath the High Atlas a small lithospheric thinning of ~10 km is imposed and a weaker plastic rheology is applied (see Table 1 for details). These small weaknesses correspond to the inherited early-Mesozoic rifting and its later inversion forming the Atlas Mountains (de Lamotte et al., 2008; Favre et al., 1991).

The last lithospheric domain corresponding to the West African Craton has a thickness of 140 km and a stronger rheology (see Table 1 for details).

The spatial resolution of the simulations varies between 10 km for those elements in the lateral and lower parts of the modelling domain, to 2 km for those elements in its upper central part of the domain. The mechanical boundary conditions are free-slip in the entire boundary. Tectonic convergence is imposed by a fixed velocity of 2 mm yr^{-1} applied to the lithosphere at each side of the model and in the regions marked in Fig. 2. These boundary conditions result in a total shortening of 4 mm yr^{-1}, which is in agreement with the estimations based on paleomagnetic fields (Argus et al., 1989), previous numerical models (Jiménez-Munt and Negredo, 2003) and from GPS data (Calais et al., 2003). Temperature is fixed at the surface (0 °C) and at the bottom of the model (1607 °C at 660 km

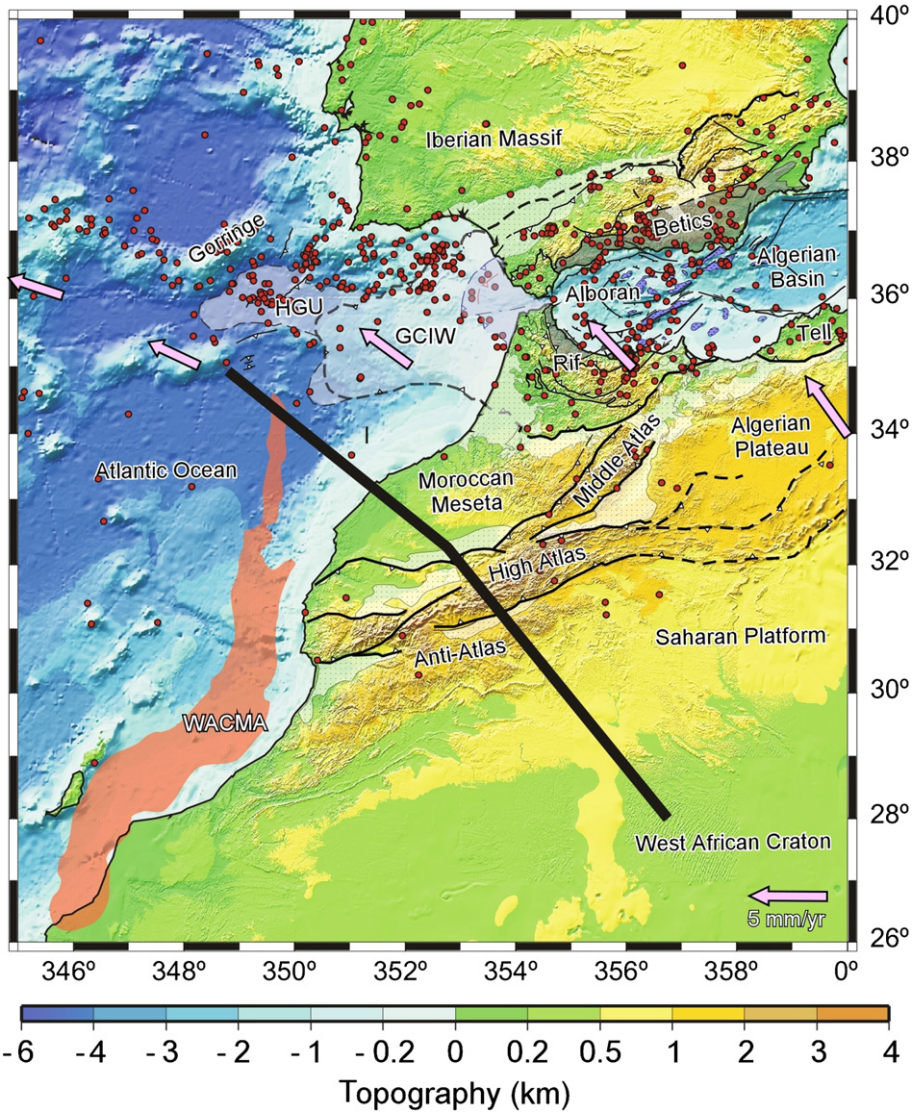

Fig. 1. The thick black line is the position of the profile in Jiménez-Munt et al. (2011). Arrows show the relative motion between Africa and Eurasia. HGU, horseshoe gravitational unit; GCIW, Gulf of Cadiz imbricate wedge; WACMA, West African coast magnetic anomaly.

depth) and null heat flow across the lateral boundaries of the model is imposed. The initial thermal field is computed as piecewise linear functions based on the top and bottom boundary conditions and a fixed temperature (1330 °C) in the LAB. The obtained averaged thermal gradients are ~12 °C km^{-1} for the lithosphere and ~0.51 °C km^{-1} for the sublithospheric mantle.

Mantle rheology (lithosphere and underlying upper mantle) follows a combination of diffusion and dislocation power-laws corresponding to wet olivine. The viscosity η_v, is computed as

$$\frac{1}{\eta_v} = \frac{1}{\eta_{disl}} + \frac{1}{\eta_{diff}}.$$

The viscosity corresponding to each power-law, is expressed as

$$\eta(T, p, \dot{\varepsilon}) = A^{-1/n} \dot{\varepsilon}^{(1-n)/2n} exp\left(\frac{E + pV}{nRT}\right)$$

where T, p and $\dot{\varepsilon}$ are the temperature (K), pressure (Pa) and strain rate (s^{-1}), respectively. The parameters are the pre-exponential parameter (A), the activation energy (E), activation volume (V) and the stress exponent (n). Values of these parameters for diffusion and dislocation creep are taken in agreement with laboratory experiments (Hirth and Kohlstedt, 2003) (see in Table 1 for details).

As usual in dynamic models a viscosity cut-off is imposed for very low temperatures and pressures. Moreover, for stresses above the yield stress, the flow law switches to a plastic behaviour. The nonlinear effective viscosity along the plastic deformation behaviour is given by

$$\eta_{yield} = \frac{\tau_{yield}}{\dot{\varepsilon}_{II}}$$

where $\tau_{yield} = \sigma_o + \alpha\, z$ (see Table 1) is the yield stress determined from Byerlee's frictional law (Byerlee, 1978; Moresi and Solomatov, 1998; Moresi et al., 2003) and $\dot{\varepsilon}_{II}$ is the second invariant of the strain rate tensor. See Table 1 for details of the rheological parameters.

Mantle density is computed linearly based on temperature and pressure, assuming a compressibility coefficient of 10^{-5} MPa^{-1} and a thermal expansivity of 3×10^{-5} K^{-1}. Mantle thermal conductivity is based on the empirical formula provided by Hofmeister (1999).

Density, viscosity and thermal conductivity for crustal bodies are considered to be independent on pressure and temperature (see Table 1 for values). As it will be seen in the following Section, the upper crust is not playing a major role during the dynamic evolution

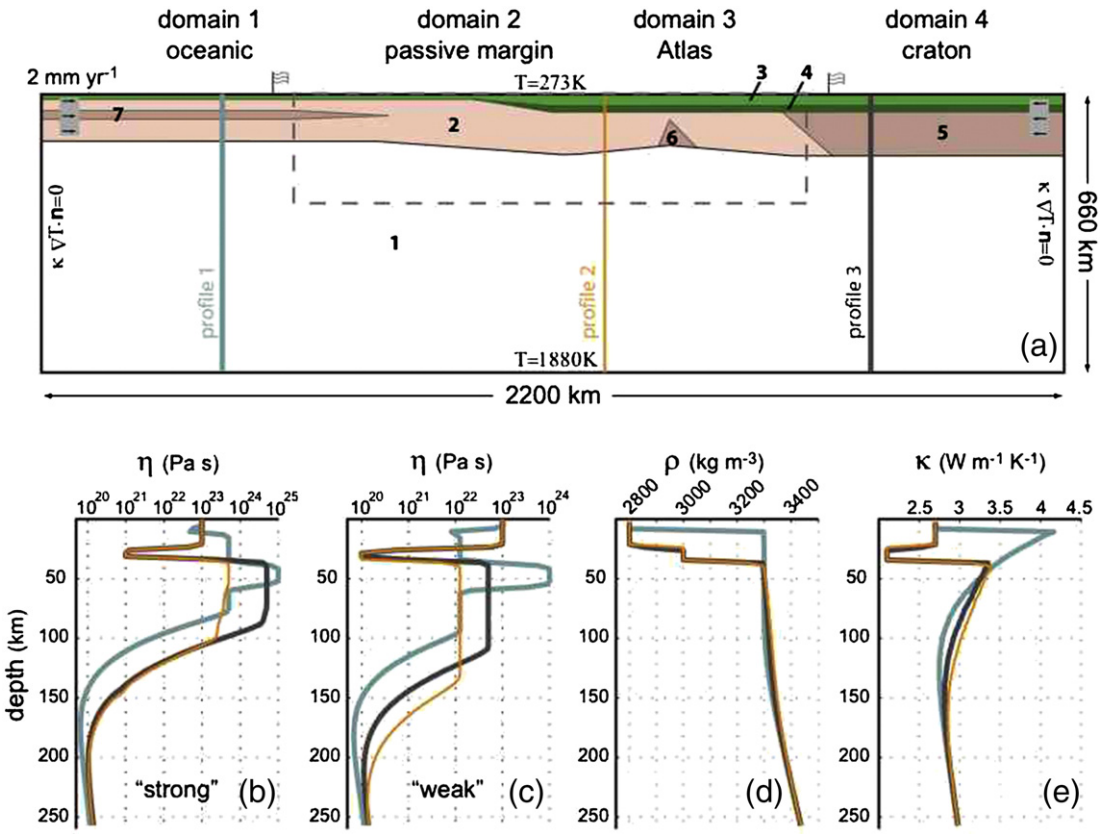

Fig. 2. Initial model setup and material property profiles. Panel *a* shows the materials forming the four different domains (bold numbers indicate different bodies: 1—upper mantle, 2—lithospheric mantle, 3—upper crust, 4—lower crust, 5—cratonic lithospheric mantle, 6—weakened lithospheric mantle, 7—strong lithospheric core). Mechanical boundary conditions are free slip on the boundary and a velocity is imposed in the two grey boxes shown in panel *a*. The dashed rectangle indicates the area of the domain shown in the next section. The two flags on the surface are pinned to the materials. They are used to estimate the crustal and mantle shortening by computing the distance between them. Lower panels display three profiles with material properties in the oceanic, continental and cratonic domains down to 250 km depth. Panels *b* to *e* show, respectively, viscosity of the "strong" models (Pa s), viscosity of the "weak" models (Pa s), density (kg m^{-3}) and thermal conductivity (W m^{-1} K^{-1}). Density and thermal conductivity are representative of all the models. Note that plotted viscosity profiles correspond to values in the models and are not computed based on a constant strain rate.

and, therefore, setting its properties constant has negligible influence on the models. On the other hand, the lower crust acts as a decoupling layer between the upper crust and the lithospheric mantle and its viscosity may have some influence. Nevertheless, the rheology of the continental lithospheric mantle is a key ingredient strongly controlling the dynamics of the process. Therefore, two end-members, one with a strong rheology (high lithospheric viscosities with respect to the underlying mantle) and one with weak rheology (lithospheric viscosities comparable with the upper mantle) are considered in the next section. Fig. 2 shows examples of viscosity profiles for the oceanic, continental and cratonic domains for the strong models (panel a) and the weak model (panel b).

Finally, radiogenic heat production is included in the energy balance equation, with values 1 μW m^{-3} for the whole crust and 0.02 μW m^{-3} for the mantle (Vilà et al., 2010).

Melting is computed as a post-process of the numerical experiments using the model of Katz et al. (2003). The degree of melting is based on temperature and pressure and assumes water content in the mantle of 200 wt ppm and a mantle composition with 0.15 modal clinopyroxene (Stixrude and Lithgow-Bertelloni, 2007).

Table 1
Rheology parameters.

Property		Units	Values	
Wet olivine creep[a]			Diffusion	Dislocation
Stress exponent, n		–	1	3.5
Activation energy, E		kJ mol^{-1}	335	480
Activation volume, V		J MPa^{-1} mol^{-1}	7	11
Pre exponential param, A		MPa^{-n} s^{-1}	1e6	90
Lithosphere plasticity				Atlas
Cohesion, σ_0		MPa	3.5	3.5
Friction angle, α		MPa km^{-1}	0.3	0.15

		Upper crust	Lower crust	Craton and oceanic core	cut-off mantle viscosity
Viscosities	Strong	10^{23}	10^{21}	10^{25}	10^{24}
η [Pa s]	Weak	10^{23}	10^{20}	10^{24}	2.5×10^{22}
Densities, ρ [kg/m^3]		2800	3000	T and P dependence	
Thermal conductivity K [W m^{-1} K^{-1}]		2.7	2.1	Hofmeister (1999)	

[a] Hirth and Kohlstedt (2003).

3. Modelling results

In this section we study the physical feasibility of the drip and drag mechanism and its capabilities to generate a lithospheric structure compatible with that currently observed in the NW-Moroccan margin and Atlas Mountains.

3.1. The drip and drag mechanism

The two main experiments corresponding to strong and weak lithospheres, respectively, reproduce the drip and drag mechanism. Nevertheless, the deformation mechanisms acting in each case are different and therefore, the evolution and the resulting lithospheric structure differ. We first describe the overall behaviour of these two experiments; details and figures are presented in Sections 3.2 and 3.3.

On one hand, experiments with a strong lithosphere have a two-stage evolution. During the first stage, the passive margin gets thicker by the regional convergence, while no deformation is occurring on the continent. The second stage starts gradually when the thickened area becomes gravitationally unstable, triggering a dripping process. The forces exerted by the drip on the continental mantle are enough to overcome its plastic yielding. These forces cause the lateral movement of a large block towards the mantle drip and consequently produce a thinned area under the Atlas (behind the moving block).

On the other hand, experiments with a weak lithosphere show simultaneous thinning beneath the continental domain and thickening in the passive margin. A large upper-mantle convection cell, involving the passive margin and the Atlas region, enhances the lithospheric thickening of the margin (in addition to the regional compressional tectonics), and produces the lithospheric thinning beneath the Atlas Mountains. Plasticity is not playing any major role when the lithosphere is weak.

A common feature of the early evolution of all the numerical experiments is the localization of deformation in the passive margin as a consequence of the regional compressive tectonics. In all experiments the passive margin gets thicker, leaving the rest of the lithosphere almost undeformed. It is worth noting that this is not numerically imposed, but arises self-consistently from the model setup. The localization of deformation is produced by a minimum in the integrated lithospheric strength in the oceanic side of the passive margin. This minimum results from a combination of the viscosity structure, the initial LAB topography and the crustal geometry.

The detailed evolution of the experiments with strong and weak lithospheres is presented below. As usual in numerical modelling, the time of the numerical experiments starts at zero in the beginning of the simulation and increases as time advances (opposite to the usual geological time convention).

3.2. Strong lithosphere

The evolution of the strong lithosphere experiment is shown in Fig. 3. The rheology of the lithospheric mantle is determined by the parameters summarized in Table 1 (combined diffusion and dislocation creep laws for olivine depending on temperature, pressure and strain rate), and a maximum cut-off viscosity of 10^{24} Pa s. The viscosity in the lower crust is 10^{21} Pa s, while in the craton and the oceanic core is 10^{25} Pa s.

The high strength of the lithosphere allows transmitting stresses over long distances favouring the localization of deformation within the passive margin over a region ~200 km wide. This localization is evidenced by the concentration of low viscosities in a relatively narrow band (see Fig. 3e). The initial lithospheric weakness under the High Atlas is not playing a noticeable role as shown by the continuity of stresses across this region and the parallel streamlines in Fig. 3b.

The thickening of the passive margin continues during ~50 My, the LAB reaching a depth of ~230 km. During this period the region beneath Atlas Mountains remains almost undeformed. The second stage of the evolution starts between 50 and 60 My as the negative buoyancy of the thickened area overcomes the viscous forces and mantle downwelling starts. The mantle drip separates the oceanic and continental lithosphere domains and the differences in their respective strengths lead to an asymmetric process concentrating the deformation on the continental side. The dragging forces exerted by the mantle drip are transmitted to the Atlas region increasing the stress up to the yielding value and therefore, activating plasticity. A large block of

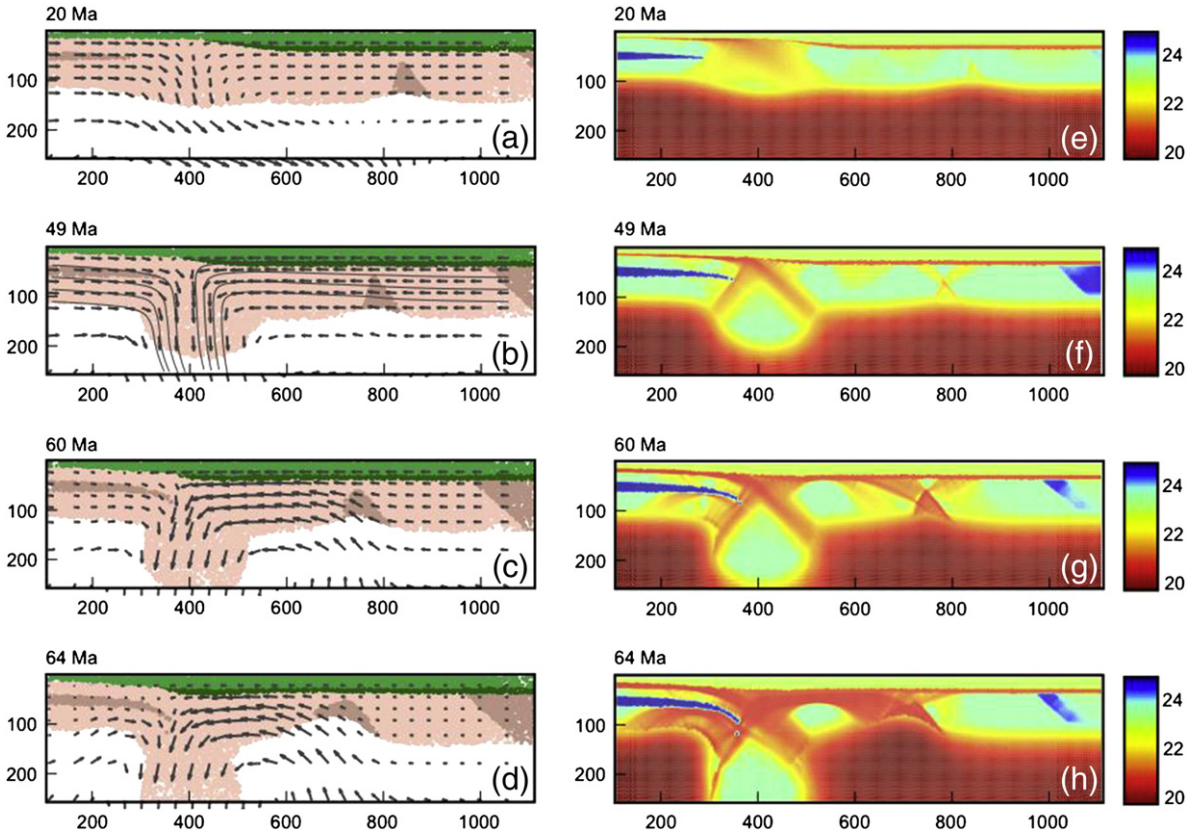

Fig. 3. Model evolution for the strong-lithosphere case. Left panels: evolution of the material position. Right panels: evolution of the viscosity field (viscosity in logarithmic scale). Panel b includes some streamlines corresponding to the velocity field at that particular time. Horizontal distances and depths are expressed in km. See caption of Fig. 2 to identify different materials.

lithospheric mantle material occupying the region between the margin and the High Atlas is then released and moves laterally towards de dripping zone at horizontal velocities of 7–9 mm yr^{-1} (Fig. 3c). Notice that these velocities are ~4 times larger than the imposed convergence on the right side of the model (2 mm yr^{-1}). At this time evolution the block maintains its mechanical coherence as inferred from its high viscosity (Fig. 3g). The lower crust acts as a detachment level, decoupling the movement and deformation of the upper crust from the lithospheric mantle. This effect is evidenced by the differences in the velocity field (Fig. 4). We measure the level of detachment as the ratio between the uppermost mantle and upper crust velocities. Then, the area comprised between the passive margin and the Atlas Mountains (the moving block) is highly decoupled, the mantle moving 70% faster than the crust. However, farther SE in the cratonic domain, the mantle velocity is 14% slower than in the crust. In the oceanic domain, as there is no lower crust, there is no appreciable crust–mantle decoupling.

The decoupling between the upper crust and the lithospheric mantle is also evidenced by the different amounts of shortening suffered by these layers. From the experiments, the shortening is computed as the variation of the distance between the flags shown in Fig. 2a. After 64 My of evolution, the upper crust accommodates a shortening of ~200 km while the mantle accommodates ~295 km indicating a difference between the average velocities of each layer of ~1.56 mm yr^{-1}.

Dynamic topography is calculated as a post-process of the resulting stress field, using the relation $\sigma_{zz} = \rho g h$, where σ_{zz} is the resulting vertical stress at surface, ρ is the upper crust density, g is the gravity and h is the topography. The calculated time-evolution of the topography in the Atlas region is shown in Fig. 5. Note that, as the experiments evolve, the location of the Atlas is not fixed in space. Here we correct this effect by locating some passive markers (moving with the materials but not having any dynamic influence) and computing the topography on top of them. Uplift in the Atlas region occurs only during the latest million years of evolution producing a maximum elevation of ~2000 m.

In the final stages (last ~15 My) of the experiment with strong lithosphere a large amount of decompression melting is produced under the thinned Atlas. At the end of the simulation melt ranges from ~1% at ~60 km depth to >10% at 100 km depth. It should be noted that, as the melting is computed as a post process, depletion effects or temperature feedback effects are not accounted and therefore, the provided values overestimate the real degree of melting.

3.3. Weak lithosphere

The other end-member experiment consists in a weak lithosphere where viscosities are between one and two orders of magnitude larger than in the asthenospheric mantle (~10^{20} Pa s at the LAB). In this case, viscosity is calculated using the same power laws and parameters as in the previous case, but now imposing a cut-off viscosity value of 2.5×10^{22} Pa s (see Table 1). The viscosities of the lower crust (10^{20} Pa s), craton (10^{24} Pa s), and strong oceanic core (10^{24} Pa s) are

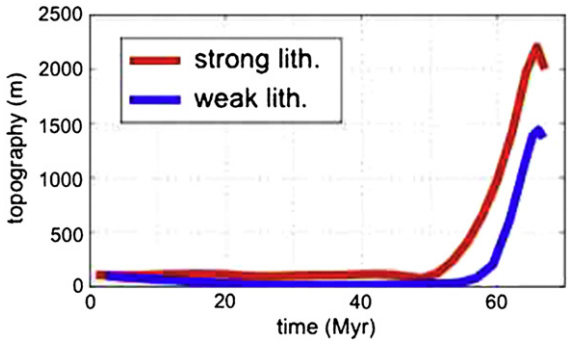

Fig. 5. Time-evolution of the dynamic topography in the Atlas region for strong-lithosphere and weak-lithosphere cases. Uplift occurs only during the last ~15–8 Ma of the evolution of both experiments, coinciding remarkably well with the geological estimations (see text for references).

lowered accordingly. All other parameters, including geometry and boundary conditions are kept as in the previous case.

The evolution of this experiment during the first 20 My shows a slow thickening of the passive margin, similar to that observed in the strong lithosphere case. The deformation nevertheless, occurs mostly by pure shear and thickening spreads over a wider area (see Fig. 6e and its differences with Fig. 3e).

After this time-step, the region beneath the Atlas gradually deforms due to gravitational instabilities. The relative low viscosities allow for the development of a Rayleigh–Taylor instability much earlier than in the previous experiment. In this case the displacement velocity is comparable in magnitude with the global convergence, resulting in a combined velocity field in which both processes interact with each other. Deformation takes place simultaneously in the passive margin and in the Atlas Mountains. Streamlines in Fig. 6b show the combination of the instabilities with the global compressive regime (compare with parallel streamlines in Fig. 3b).

After 35 My the evolution continues with a similar trend characterized by a large convective cell with its upwelling flow beneath Atlas and its downwelling flow beneath the passive margin, thus contributing to the development of both, lithospheric thinning and thickening. The shallower part of this convective cell moves lithospheric mantle material horizontally towards the passive margin. Velocity arrows shown in Fig. 6c and d illustrate the interaction between the convective cell and the imposed shortening.

The resulting lithospheric structure after 50 My is very similar to that proposed by Jiménez-Munt et al. (2011) for the present-day. The lower crust in the weak-lithosphere case also acts as an effective decoupling level. In the margin region the mantle velocities are 36% larger than those in the upper crust. Although the average velocities obtained in this model (2 to 3 mm yr^{-1}) are slower than in the strong experiment, the lithospheric thinning in the Atlas region occurs more rapidly than in the strong model. This is because deformation starts

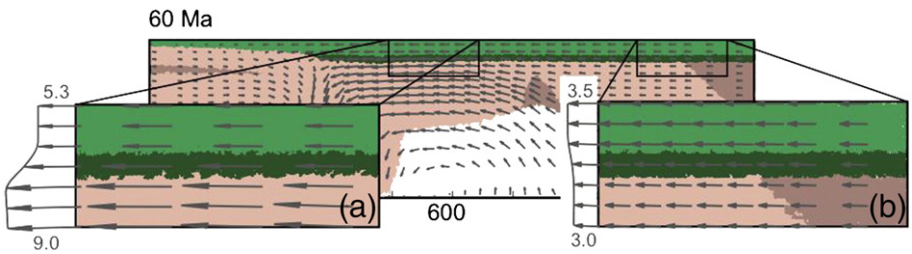

Fig. 4. The velocity field for the strong-lithosphere case at 60 Ma illustrates the degree of decoupling between the upper crust and the lithospheric mantle. Panels *a* and *b* show a blow-up of the velocity field in the NW and SE flanks of the Atlas region. Grey numbers denote velocities in mm yr^{-1}. The variation of velocities between the upper crust and the lithospheric mantle is ~70% in the NW flank and ~16% in the SE flank. See caption of Fig. 2 to identify the different materials.

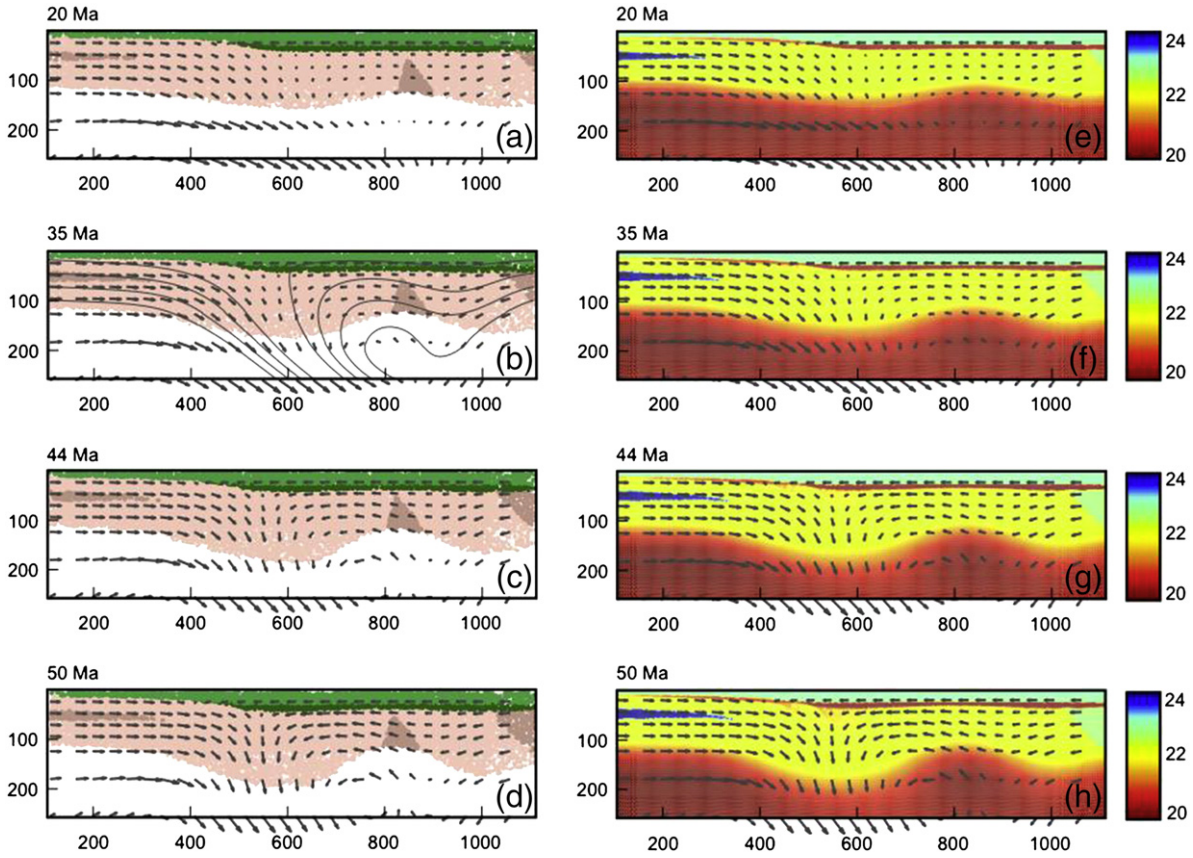

Fig. 6. Model evolution for the weak-lithosphere case. Left panels: evolution of the materials position. Right panels: evolution of the viscosity field (viscosity in logarithmic scale). The lithospheric structure at 50 Ma is very similar to those proposed in Zeyen et al. (2005), Jiménez-Munt et al. (2011), Teixell et al. (2005) and Missenard et al. (2006). Panel b includes some streamlines corresponding to the velocity field at that particular time. Horizontal distances and depths are expressed in km. See caption of Fig. 2 to identify different materials.

much earlier due to the weaker rheology. The shortenings undergone by the crust and mantle are in this case of 158 and 166 km, respectively thus indicating a more coupled system than in the previous experiment.

The evolution of the dynamic topography in the Atlas region (Fig. 5) follows a trend similar to the strong-lithosphere case, although maximum highs are lower and uplift starts later in time. The elevation along the transect generated by the two numerical experiments is shown in Fig. 7, together with the actual elevation obtained from GINA Topo Data (Lindquist et al., 2004) along the profile modelled by Jiménez-Munt et al. (2011) from the NW Moroccan margin to the West African Craton (Fig. 1).

The melt production in this experiment is more modest than in the previous case (with strong lithosphere). Nevertheless, decompression melting is observed in the last ~10 My of the evolution of the experiment. At its end, ~1% of melt is observed at 70 km depth and ~7% at 70 km depth.

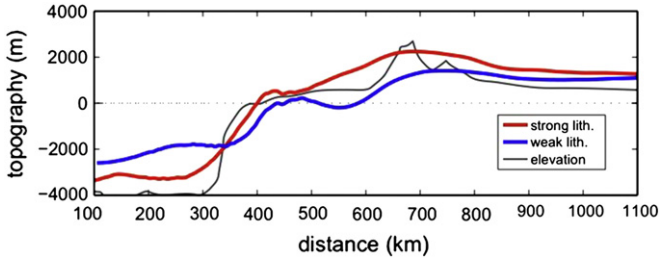

Fig. 7. Topography along the transect calculated from numerical experiments and actual elevation derived from GINA Global Topo Data (Fullea et al., 2007, 2010; Lindquist et al., 2004; Missenard et al., 2006; Teixell et al., 2005).

3.4. Influence of the main structural units

In the previous sections we have shown examples of the drip and drag process in a simplified model of the Moroccan Margin and Atlas Mountains. The model includes some major structural units, such as the West African Craton or the weakened zone in the Atlas region. In this section we analyse how the presence of these structural units may modify the resulting crust and mantle flow.

3.4.1. Influence of the craton

The drip and drag process is not much affected by the presence or absence of the craton. In the strong lithosphere case, the absence of the craton results in minor differences in the elevation (<300 m) and in the degree of coupling between the upper crust and the lithospheric mantle. In the weak lithosphere case, the absence of the craton does not prevent the drip and drag process to develop and the final lithospheric structure is very similar to the case in which the craton is considered. Nevertheless, during the initial compressive stage, the weak lithospheric mantle suffers pure shear deformation, increasing its thickness and delaying the thickening of the passive margin.

3.4.2. Influence of the oceanic strong core

The presence of the strong core is essential for the asymmetric development of the instability. The strong core causes a noticeable difference between the integrated strength of the oceanic and continental lithospheres and, consequently, it is responsible for the one-sided drag process. The Rayleigh–Taylor instability in the experiments without

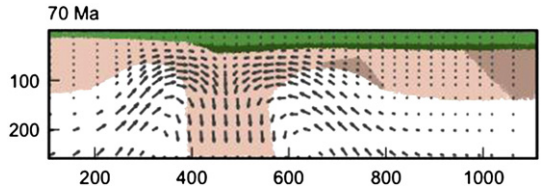

Fig. 8. Snapshot of the material position at 70 My resulting from the experiment without strong core in the oceanic lithosphere. In this case the instability is resolved as a symmetric Rayleigh–Taylor process. Horizontal distances and depths are expressed in km. See caption of Fig. 2 to identify different materials.

the strong core is almost symmetric (Fig. 8) and the resulting deformation pattern is very similar to that obtained by Göğüş and Pysklywec (2008), and by Harig et al. (2010). A minor asymmetry is caused by the presence of the weak zone beneath the Atlas, increasing slightly the lateral extension of the deformation in the continental side.

3.4.3. Influence of the initial LAB geometry

In all previous numerical experiments, the initial LAB has a geometry corresponding to a mature passive margin. The lithospheric thickness has important influence on the dynamics since it determines the integrated lithospheric strength and, on the other hand, any lateral variation in thickness induces flow in the mantle. The initial step of the numerical experiments presented here corresponds to approximately 60 Ma, so it is difficult to have accurate estimations of the LAB topography at that time. To overcome this uncertainty we explore the behaviour of the model in two end member cases: one with an initially flat LAB, with a constant lithospheric thickness of 110 km in all the domains, and another with an initially thickened passive margin.

Interestingly the model with a flat LAB does not reproduce the drip and drag process. Instead, it results in a delamination of the oceanic lithosphere (Fig. 9). During the initial 45 My, this model evolves similarly to previous cases: the passive margin thickens and the Atlas region does not undergo any deformation. Gradually between 45 and 50 My, the thickened area in the margin becomes gravitationally unstable but, in this case, the instability does not lead to a Rayleigh–Taylor process but

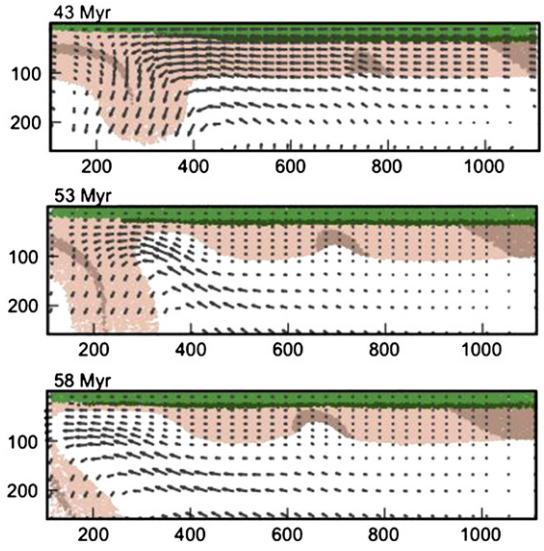

Fig. 9. Evolution of the material position resulting from the experiment with an initial flat lithosphere–asthenosphere boundary. In this case the drip and drag process is not produced. Instead, a lithospheric delamination of the oceanic lithosphere is observed. The deformation of the Atlas region only starts when the delamination is active. The resulting lithosphere structure differs noticeably from that proposed by Jiménez-Munt et al. (2011). Horizontal distances and depths are expressed in km. See caption of Fig. 2 to identify different materials.

results in a delamination of the oceanic lithosphere. The main reason for this difference is the degree in which the oceanic strong core is inserted into the thickened area. When the gravitational instability develops, the core transmits stresses to the oceanic lithosphere avoiding the detachment of the drip. This delamination is very similar to those observed in other numerical studies (e.g., Afonso and Zlotnik, 2011; Duretz and Gerya, 2013). Only once the delamination process has started, the Atlas region is extended and the lithosphere is thinned. Actually, there is no simultaneous thickening beneath the margin and thinning beneath the Atlas at any stage of the model evolution.

The other end-member, in which we consider an initially thickened margin develops the drip and drag process more rapidly. At ~28 My the LAB topography is very similar to those proposed in Jiménez-Munt et al. (2011).

3.4.4. Influence of the lithospheric weakness beneath the Atlas

The lithospheric weakness beneath the Atlas, imposed by a region with a slightly weaker plastic law, is not a key feature for the drip and drag process to develop. Even when this weakness is not present the asymmetric process evolves very similarly to previous cases. Only in the strong-lithosphere case some effects are noticeable in: i) defining the location of the thinned area (the lithospheric thinning is closer to the drip if the weakness is not present), and ii) delaying the occurrence of deformation in time. In the weak-lithosphere case plasticity is not important and therefore the existence of this weakness region is negligible.

3.4.5. Influence of the convergence velocity

Finally, we tested the effect of the imposed convergence velocity on the resulting mantle flow. In this new experiment we considered that the convergence velocity of 2 mm yr^{-1} applied to each side of the model was acting only during the first 45 My. During this period, the lithospheric mantle beneath the continental margin thickens as in previous experiments. After this time, we remove the velocity constraints and left the oceanic plate to move free while the continental plate is pinned at the right tip of the modelling domain. The resulting evolution differs substantially from all the previous tests (Fig. 10). After releasing the oceanic plate, a drip similar to those observed in previous models starts forming. Note that the resulting velocity field is asymmetric in shape but, in contrast to previous cases, the magnitudes of the involved velocities are very symmetric (Fig. 10b). It is worth noting that the generated mantle drip does not evolve as Rayleigh–Taylor instability, but triggers the generation of a new subduction zone. The oceanic lithosphere continues subducting for >20 My, it is consumed. During the subduction process, the sub-continental mantle lithosphere is dramatically thinned resembling typical lithosphere delamination geometry.

4. Discussion

4.1. Lithospheric structure and dynamic models

Based on gravity, geoid, elevation, heat flow and crustal structure, Jiménez-Munt et al. (2011) propose a lithospheric structure for the Moroccan Margin where the passive margin is thickened with the LAB exceeding 200 km depth, while the lithosphere beneath the Atlas is thinned. To explain the existence of this unusual configuration they propose a geodynamic process based on the generation of a gravitational mantle drip (Rayleigh–Taylor instability) combined with the lateral drag of lithospheric mantle. The drag would displace lithospheric material horizontally, thus contributing to the development of both the thinned and the thickened areas (Fig. 11). Differently from a usual Rayleigh–Taylor instability, the asymmetric drag can help in the formation of such a structure, concentrating the deformation in only one side of the drip. Our numerical study shows that a lithospheric drip combined with a lateral drag process is physically feasible and that the

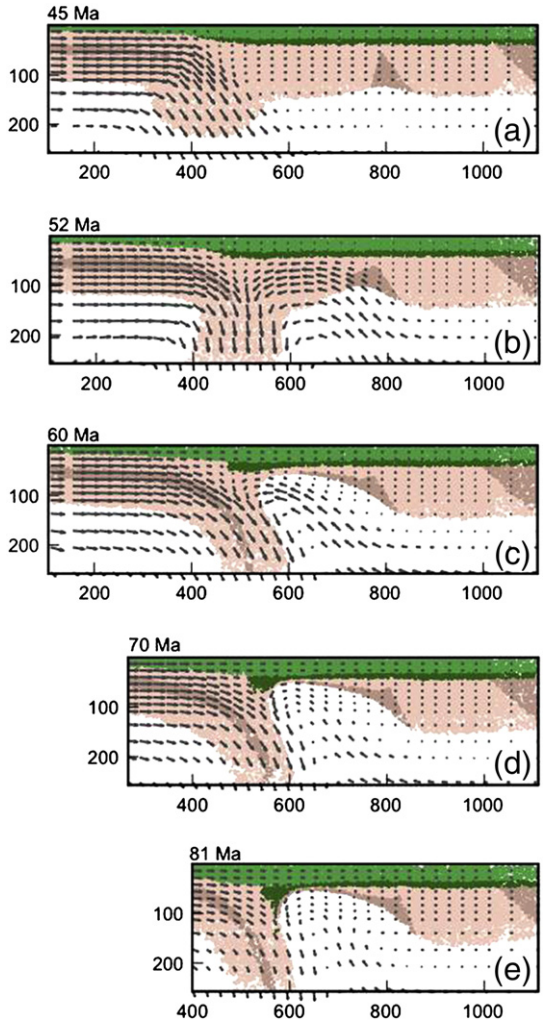

Fig. 10. Evolution of the material position resulting from the experiment with free oceanic plate. In this case a new subduction zone is formed and becomes active until all the existent oceanic lithosphere is consumed. The evolution previous to 45 Ma corresponds exactly with the strong-lithosphere case and is not shown. Horizontal distances and depths are expressed in km. See caption of Fig. 2 to identify different materials.

geodynamic setup of a passive margin under compression, such as the NW-Moroccan margin, is appropriate for this kind of process to develop.

The mantle drip and asymmetric drag mechanism is particularly suitable along the studied profile but needs the interaction with other geodynamic processes to explain the complex evolution of the region. Fullea et al. (2010) propose that the Atlantic–Mediterranean transition region (Betic–Rif system, NW-Moroccan margin and Atlas domain) resulted from four different processes including: i) protracted Africa–Eurasia convergence; ii) compression in the Betic–Rif system due to slab roll-back, iii) back-arc extension in the Alboran and Algerian basins; and iv) small-scale convection or 'baby' mantle plume along the Atlas domain. Verges and Fernández (2012) proposed a kinematic evolution for the Betic–Rif system based on the NW and W retreating of an initially SE-dipping Tethyan slab, which generated the Betic–Rif orogenic arc and the extended Alboran basin in the back-arc and favouring a N-directed mantle flow from the Middle Atlas to the Alboran Basin. Therefore, the drip and drag mechanism would be limited to the NE by the Betic–Rif orogen being the SW limit more uncertain but probably restricted to the W-Atlas (Jiménez-Munt et al., 2011).

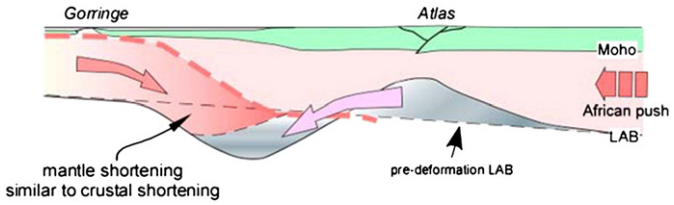

Fig. 11. Cartoon showing the proposed drip and asymmetric lateral dragging to be acting in the NW-Moroccan margin and Atlas Mountains to explain the present-day lithosphere configuration according to Jiménez-Munt et al. (2011).

The presented numerical experiments are based on simplified models with the main aim of testing the feasibility of the process. Therefore the goal is far to reproduce exactly the observables of any particular region, but to understand the operating processes and gain insight on them. Moreover, it makes little sense trying to tune the observables inferred from steady-state models with dynamic models in which the knowledge on rheology, and applicable initial and boundary conditions show large uncertainties. Taking that into account, the main trends of the observables obtained from the numerical experiments match remarkably well with the geological and geophysical observations in the NW-Moroccan margin.

Developing drip and asymmetric drag processes needs the following ingredients:

1. Initiation: a compressive tectonic setup favouring a locally thickened lithospheric mantle that will trigger the mantle drip.
2. Asymmetry: different lithospheric strength at each side of the thickened area. In our case, the passive margin reproduces this asymmetry, as the lithospheric strength of the oceanic and continental lithospheres differs noticeably.
3. Thinning: the drip and asymmetric drag process generates a region of lithospheric mantle thinning adjacent to the drip. Nevertheless, if a lithospheric weakness is nearby (for example an aborted rift), the location of the thinned area can displace to the weak zone, enlarging the dragged area.
4. Subduction: in our passive margin context, the oceanic lithosphere cannot move freely during the development of the drip and drag process. However, if the oceanic plate is allowed to move free during the dripping process, then subduction develops.

In addition to these requirements, the numerical experiments show that the process is reasonably robust relative to the lithospheric rheology and it may develop in a wide range of viscosity values. However, the dynamics of the process is different depending on the strength of the lithosphere. Strong lithospheres favour crust–mantle decoupling and produce slightly higher topography. Weak lithospheres accelerate the process and produce lithospheric structures resembling that proposed in Jiménez-Munt et al. (2011).

4.2. Topography

The Atlas Mountains are approximately 100 km wide and have an average elevation of 2000 m with maximum values exceeding 4000 m in the High Atlas. The tectonic shortening of the Atlas during Cenozoic is small, ranging from 15% to 24% in the High Atlas and less than 10% in the Middle Atlas (Arboleya et al., 2004; Beauchamp et al., 1999; Gomez et al., 1998; Teixell et al., 2003, 2005). The maximum crustal thickness inferred from Contrucci et al. (2004) and Teixell et al. (2005) is ~40 km being insufficient to explain the elevation of the Atlas Mountains and therefore, a second uplift mechanism is needed. Moreover, the Atlas Mountains are surrounded by peripheral plateaus in which the average elevation is above 1200 m (Babault et al., 2008). These observations support the idea of a long-wavelength, mantle-related uplift. Several of such mechanisms have been proposed in the literature to explain the Atlas elevation involving thinned or delaminated lithospheric mantle, e.g. (de Lamotte et al., 2008; Fullea et al., 2010; Jiménez-Munt et al., 2011; Seber et al., 1996; Teixell et al., 2005).

The elevation predicted by our numerical experiments (Fig. 7) has comparable trends with the current topography, with its maximum located on top of the High Atlas. The wavelength of the predicted elevation is larger than the width of the Atlas Mountains but similar to the region including the surrounding plateaus. Taking into account that the models do not reproduce the localization of the crustal shortening in the Atlas (due to the space scale and the simplified crustal rheology), it is not expected to reproduce the elevation related with crustal processes. However, the numerical experiments tend to systematically overestimate the elevation in the cratonic domain due to the biassing effect of the imposed velocity boundary conditions.

A remarkable result from our numerical experiments is the rates and ages of the Atlas uplift, which vary from 0.13 to 0.2 mm yr^{-1} and 8 to 15 Ma, respectively and coincide pretty well with observations. Babault et al. (2008) propose uplift rates of 0.17 to 0.22 mm yr^{-1} based on uplifted Messinian shallow deposits, tilted lacustrine deposits and drainage-network reorganization in the Middle–High Atlas region. These authors also establish a total uplift of around 1000 m of large wavelength and deep origin occurring since 7.1 to 5.3 Ma. Other authors proposed similar or slightly older ages for the Atlas uplift based on AFT data. Then, Missenard et al. (2008) propose AFT ages ranging between 27 and 9 Ma for the High Atlas; Barbero et al. (2007) and Barbero et al. (2011) propose, based on AFT and sedimentary data, an uplift age younger than 20 Ma for the central High Atlas and Western Moroccan Meseta and finally, Balestrieri et al. (2009) proposed a Middle–Late Miocene age for the South Atlas Fault Zone.

On the passive margin and oceanic domain the predicted elevation is shallower than the actual bathymetry (Fig. 7). To this respect it must be considered that our numerical experiments do not include marine sediments which amount several kilometres in thickness. Nevertheless, some common trends as the position of the coast-line and the continental slope are well reproduced. Finally, our numerical experiments predict a subsidence rate that keeps almost constant with time differing notoriously from the time-exponential decrease of tectonic subsidence observed in many passive margins. Unfortunately there are no available studies on the tectonic subsidence of the NW-Moroccan margin that can validate or contradict these results.

4.3. Shortening & crust–mantle decoupling

The total crustal shortening estimated along the transect is approximately of 60 km, divided in 13–30 km in the Atlas (Teixell et al., 2003), 10–20 km between the Gorringe Bank and the coastline (Zitellini et al., 2009), and more that 20 km in the Gorringe Bank (Galindo-Zaldívar et al., 2003; Jiménez-Munt et al., 2010). The estimated displacement of Africa relative to Eurasia is ~150 km during the last 55 My, as derived from plate kinematic reconstructions (Rosenbaum et al., 2002). This amount of convergence differs considerably from the estimated crustal shortening, implying a larger accommodation at crustal scales either farther NW of the Gorringe Bank or off the strike of the profile, or a combination of both.

This shortening paradox indicates a strong decoupling between crust and mantle, which is very well reproduced in the numerical experiments. Particularly, in the region where the drag process is active, the mantle velocities reach values four times larger than crustal velocities. Decoupling is also evident in the experiments in the different shortenings suffered by crust and mantle (Fig. 4). In the region where the lithospheric thinning occurs, the decoupling between crust and lithospheric mantle is even more dramatic: the crust has a shortening of 25%, while the lithospheric mantle suffers extension values increasing with depth, ranging from 30% on the shallow mantle, to >200% at LAB depth.

Despite in our models crustal deformation is extremely simplified the large variations in the lithospheric mantle thickness contrast with the more homogeneous crustal structure. These differences in the crust and lithosphere mantle geometries indicate that the convergence in this segment is dominated by crust-mantle strain partitioning. Decoupling between crust and mantle is also evidenced by the contrasting widths of the regions over which crust and mantle shortening are accommodated (Figs. 3 and 6). Whereas crustal shortening is accommodated almost homogeneously over the whole region, most of the lithospheric mantle shortening is absorbed between the continental margin and the Atlas Mountains over a ~400 km wide region. This effect is also observed in the velocity decoupling between the upper crust and lithospheric mantle, and how it changes along the profile (Fig. 4).

4.4. Decompression melting and volcanism

Volcanic activity of alkaline intraplate chemical affinity took place in the Atlas Domain from Miocene to Pliocene (Missenard and Cadoux, 2012) and references therein). Several hypotheses were aimed to explain its existence including lateral flow of asthenospheric material related to Mediterranean slab subduction (Teixell et al., 2005), lithospheric delamination (Duggen et al., 2009), "baby plumes" or convection cells (Fullea et al., 2010) and edge-driven convection (Missenard and Cadoux, 2012). Another possible source for these magmatic events is decompression melts due to the rapid ascent of hot asthenospheric mantle material in the thinned zone produced by the drip and drag process. Independently of the strength of the lithosphere, a relatively large degree of melt (7 to 10%) was produced in the numerical experiments. This melt source was formed in the later stages of the process (approximately last 15 My) coinciding with the dates of the observed volcanism (11 to 2.9 Ma).

In addition to the Miocene–Pliocene events, some Paleocene to Eocene volcanism is present in the Atlas Domain. The later are not reproduced in our experiments and could be related to any, or a combination, of the different processes proposed in the literature.

4.5. Dynamic evolution

Our numerical results suggest that there are three possible tectonic evolutions for a locally thickened passive margin under convergence: i) removal of thickened mantle by Rayleigh–Taylor instability (either symmetric or asymmetric), ii) total or partial removal of lithospheric mantle by delamination, and iii) creation of a new subduction zone.

Convective removal occurs when the strength of the lithospheric mantle is not enough to maintain its coherence in front of the gravitational instability. In this case the negative buoyancy produces a drop and necking and, consequently, part of the lithospheric mantle is separated from the plate and sinks into the upper mantle. The symmetry (or asymmetry) of this process is conditioned by the symmetry (or asymmetry) of the integrated strength at the sides of the thickened area.

The second and third possible evolutions (delamination/subduction) occur when the buoyant forces are transmitted to the oceanic plate. This is the usual case in a subduction zone where the slab pull induces (at least partially) the motion of plates. In our models, the strong lithospheric core is the body that transmits the forces to the oceanic plate. Depending on how deep the strong core is mechanically inserted into the thickened lithosphere, the buoyancy forces are transmitted to the oceanic plate and produce its advance towards the margin or alternatively, buoyancy forces produce necking and a Rayleigh–Taylor instability develops.

When buoyancy forces are successfully transmitted the occurrence or subduction or delamination depends on the kinematic constraints imposed at the lateral plate boundaries. Delamination needs of some kinematic restriction avoiding the plate advance to the margin. The 2D numerical experiments oversimplify boundaries by omitting the lateral sides of the plates. The motion of a full 3D plate in spherical geometry requires the accommodation of the displacements all along its boundary, usually having segments of transform faults. Therefore, even when some part of the plate boundary could be considered to move

freely (for example mid oceanic ridges), the advance of the whole plate could be restricted at other segments of the plate boundary. In that case, a mantle delamination process would take place.

Conversely, if the plate can move freely, a new subduction zone can be formed. Despite this is not a self-consistent explanation for subduction initiation (velocity boundary conditions were imposed to generate the initial thickening in the margin), it represents a plausible scenario and is supported by previous models (e.g., Erickson, 1993; Erickson and Arkani-Hamed, 2010; Faccenda et al., 2009; Nikolaeva et al., 2010; Stern, 2004).

Determining the current state of the NW-Moroccan margin is out the scope of this work. The observables predicted by our numerical experiments do not allow us distinguishing between the three proposed scenarios (gravitational instability, delamination or subduction initiation). In any case, the proposed lithospheric structure corresponds to an evolution stage just previous to the full development of any of these scenarios.

5. Concluding remarks

In this work we have studied the dynamics of lithospheric mantle instabilities in the tectonic context of a passive margin under compression and its application to the NW-Moroccan margin. The results obtained from the numerical experiments allow us to draw the following concluding remarks:

i) A mechanism of asymmetric gravitational instability producing mantle drip – and thickening – beneath the margin and lateral mantle drag – and thinning – beneath the continental domain is dynamically feasible under plausible conditions.
ii) The development of such process essentially depends on the existence of a lateral lithospheric strength variation to allow for an asymmetric evolution of the mantle dripping and lateral dragging, the latter being more effective in the weakest lithospheric domain.
iii) Other structural components that may be present, such as lithospheric weakness related to recent lithospheric extension or stiffness related to cratonic lithosphere, may have some influence on the process but play a secondary role. Their presence is not required to trigger the process and is not enough to avoid it.
iv) Depending on the kinematic boundary conditions, the further evolution of the drip and drag process can become either in convective removal and lithosphere mantle sinking into the underlying asthenosphere, or mantle delamination, or subduction initiation.
v) The drip and drag mechanism can account for the inferred present-day lithospheric structure across the NW-Moroccan margin and Atlas Mountains, the characteristic time of the observed vertical movements, the amplitude and rates of uplift in the Atlas Mountains and the Miocene to Pliocene volcanism. The model predicts an abnormal subsidence in the margin characterized by an almost constant tectonic subsidence rate that should be confirmed by observations.

Acknowledgments

This study has been financially supported by the Spanish Government through projects DPI2011-27778-C02-02; ATIZA (CGL2009-09662-BTE), TOPOMED (CGL2008-03474-E/BTE), ESF-Eurocores (07-TOPOEUROPE-FP006) and Consolider-Ingenio 2010 Topo-Iberia (CSD2006-00041). We thank J. Vergés for his fruitful discussions on the geology of the Atlas Mountains. Reviews by Y. Missenard and M. Faccenda were extremely useful. Finally, we acknowledge W.L. Griffin for editorial handling of the manuscript.

References

Afonso, J.C., Zlotnik, S., 2011. The subductability of continental lithosphere: the before and after story. Frontiers in Earth Sciences. Springer Berlin Heidelberg, Berlin, Heidelberg, pp. 53–86.
Afonso, J.C., Ranalli, G., Fernández, M., 2007. Density structure and buoyancy of the oceanic lithosphere revisited. Geophysical Research Letters 34 (10), 10302.
Afonso, J.C., Zlotnik, S., Fernández, M., 2008. Effects of compositional and rheological stratifications on small-scale convection under the oceans: implications for the thickness of oceanic lithosphere and seafloor flattening. Geophysical Research Letters 35 (20), L20308.
Arboleya, M.L., Teixell, A., Charroud, M., Julivert, M., 2004. A structural transect through the High and Middle Atlas of Morocco. Journal of African Earth Sciences 39 (3–5), 319–327.
Argus, D.F., Gordon, R.G., De Mets, C., Stein, S., 1989. Closure of the Africa–Eurasia–North America plate motion circuit and tectonics of the Gloria fault. Journal of Geophysical Research 94, 5585–5602.
Artemieva, I., 2006. Global 1° × 1° thermal model TC1 for the continental lithosphere: implications for lithosphere secular evolution. Tectonophysics 416 (1–4), 245–277.
Artemieva, I., 2011. The Lithosphere: an Interdisciplinary Approach. Cambridge University Press.
Babault, J., Teixell, A., Arboleya, M.L., Charroud, M., 2008. A Late Cenozoic age for long-wavelength surface uplift of the Atlas Mountains of Morocco. Terra Nova 20 (2), 102–107.
Balestrieri, M.L., Moratti, G., Bigazzi, G., Algouti, A., 2009. Neogene exhumation of the Marrakech High Atlas (Morocco) recorded by apatite fission-track analysis. Terra Nova 21 (2), 75–82.
Barbero, L., Teixell, A., Arboleya, M.L., del Río, P., Reiners, P.W., Bougadir, B., 2007. Jurassic-to-present thermal history of the central High Atlas (Morocco) assessed by low-temperature thermochronology. Terra Nova 19 (1), 58–64.
Barbero, L., Jabaloy, A., Gómez-Ortiz, D., Vicente Pérez-Peña, J., Rodríguez-Peces, M.J., Tejero, R., Estupiñán, J., Azdimousa, A., Vázquez, M., Asebriy, L., 2011. Evidence for surface uplift of the Atlas Mountains and the surrounding peripheral plateaux: combining apatite fission-track results and geomorphic indicators in the Western Moroccan Meseta (coastal Variscan Paleozoic basement). Tectonophysics 502 (1), 90–104.
Beauchamp, W., Allmendinger, R.W., Barazangi, M., Demnati, A., El Alji, M., Dahmani, M., 1999. Inversion tectonics and the evolution of the High Atlas Mountains, Morocco, based on a geological–geophysical transect. Tectonics 18 (2), 163–184.
Bird, P., 1978. Initiation of intracontinental subduction in the Himalaya. Journal of Geophysical Research: Solid Earth (1978–2012) 83 (B10), 4975–4987.
Byerlee, J., 1978. Friction of rocks. Pure and Applied Geophysics 116 (4), 615–626.
Calais, E., DeMets, C., Nocquet, J.M., 2003. Evidence for a Post-3.16-Ma Change in Nubia–Eurasia–North America Plate Motions? Earth and Planetary Science Letters 216 (1), 81–92.
Capitanio, F.A., Faccenna, C., Zlotnik, S., Stegman, D.R., 2011. Subduction dynamics and the origin of Andean orogeny and the Bolivian orocline. Nature 480 (7375), 83–86.
Contrucci, I., Klingelhöfer, F., Perrot, J., Bartolomé, R., Gutscher, M.A., Sahabi, M., Malod, J., Rehault, J.P., 2004. The crustal structure of the NW Moroccan continental margin from wide-angle and reflection seismic data. Geophysical Journal International 159 (1), 117–128.
de Lamotte, D.F., Leturmy, P., Missenard, Y., Khomsi, S., Ruiz, G., Saddiqi, O., Guillocheau, F., Michard, A., 2008. Mesozoic and Cenozoic vertical movements in the Atlas system (Algeria, Morocco, Tunisia): an overview. Tectonophysics 1–20.
Duggen, S., Hoernle, K.A., Hauff, F., Klugel, A., Bouabdellah, M., Thirlwall, M.F., 2009. Flow of Canary mantle plume material through a subcontinental lithospheric corridor beneath Africa to the Mediterranean. Geology 37 (3), 283–286.
Duretz, T., Gerya, T.V., 2013. Slab detachment during continental collision: influence of crustal rheology and interaction with lithospheric delamination. Tectonophysics 1–64.
Erickson, S.G., 1993. Sedimentary loading, lithospheric flexure, and subduction initiation at passive margins. Geology 21 (2), 125.
Erickson, S.G., Arkani-Hamed, J., 2010. Subduction initiation at passive margins: the Scotian Basin, eastern Canada as a potential example. Tectonics 12 (3), 678–687.
Faccenda, M., Minelli, G., Gerya, T.V., 2009. Coupled and decoupled regimes of continental collision: numerical modeling. Earth and Planetary Science Letters 278 (3–4), 337–349.
Favre, P., Stampfli, G., Wildi, W., 1991. Jurassic sedimentary record and tectonic evolution of the northwestern corner of Africa. Palaeogeography, Palaeoclimatology, Palaeoecology 87 (1–4), 53–73.
fernandez, M., Marzán, I., Torne, M., 2004. Lithospheric transition from the Variscan Iberian Massif to the Jurassic oceanic crust of the Central Atlantic. Tectonophysics 386 (1–2), 97–115.
Fernández, M., Torne, M., García-Castellanos, D., Vergés, J., Wheeler, W., Karpuz, R., 2004. Deep structure of the Vøring Margin: the transition from a continental shield to a young oceanic lithosphere. Earth and Planetary Science Letters 221 (1–4), 131–144.
Fernández, M., Marzán, I., Torne, M., 2005. Lithospheric structure of the Mid-Norwegian Margin: comparison between the Møre and Vøring margins. Journal of the Geological Society 162, 1005–1012.
Fernández, M., Afonso, J.C., Ranalli, G., 2010. The deep lithospheric structure of the Namibian volcanic margin. Tectonophysics 481 (1–4), 68–81.
Fullea, J., Fernández, M., Zeyen, H., Vergés, J., 2007. A rapid method to map the crustal and lithospheric thickness using elevation, geoid anomaly and thermal analysis. application to the Gibraltar Arc System, Atlas Mountains and adjacent zones. Tectonophysics 430 (1–4), 97–117.

Fullea, J., Fernández, M., Afonso, J.C., Vergés, J., Zeyen, H., 2010. The structure and evolution of the lithosphere–asthenosphere boundary beneath the Atlantic–Mediterranean Transition Region. Lithos 120 (1–2), 74–95.

Galindo-Zaldívar, J., Maldonado, A., Schreider, A.A., 2003. Gorringe Ridge gravity and magnetic anomalies are compatible with thrusting at a crustal scale. Geophysical Journal International 153 (3), 586–594.

Gemmer, L., Houseman, Gregory A., 2007. Convergence and extension driven by lithospheric gravitational instability: evolution of the Alpine–Carpathian–Pannonian system. Geophysical Journal International 168 (3), 1276–1290.

Göğüş, O., Pysklywec, R.N., 2008. Mantle lithosphere delamination driving plateau uplift and synconvergent extension in eastern Anatolia. Geology 36 (9), 723.

Gomez, F., Allmendinger, R., Barazangi, M., Er-Raji, A., Dahmani, M., 1998. Crustal shortening and vertical strain partitioning in the Middle Atlas Mountains of Morocco. Tectonics 17 (4), 520–533.

Harig, C., Molnar, P., Houseman, G.A., 2010. Lithospheric thinning and localization of deformation during Rayleigh–Taylor instability with nonlinear rheology and implications for intracontinental magmatism. Journal of Geophysical Research 115 (B2), B02205.

Hirth, G., Kohlstedt, D., 1996. Water in the oceanic upper mantle: implications for rheology, melt extraction and the evolution of the lithosphere. Earth and Planetary Science Letters 144 (1–2), 93–108.

Hirth, G., Kohlstedt, D., 2003. Rheology of the upper mantle and the mantle wedge: a view from the experimentalists. Geophysical Monograph—American Geophysical Union 138, 83–106.

Hofmeister, A.M., 1999. Mantle values of thermal conductivity and the geotherm from phonon lifetimes. Science 283 (5408), 1699.

Houseman, G.A., Gemmer, L., 2007. Intra-orogenic extension driven by gravitational instability: Carpathian–Pannonian orogeny. Geology 35 (12), 1135–1138.

Houseman, G., Molnar, P., 2001. Mechanisms of lithospheric rejuvenation associated with continental orogeny. Geological Society London Special Publications 184 (1), 13–38.

Houseman, Greg A., McKenzie, D., Molnar, P., 1981. Convective instability of a thickened boundary layer and its relevance for the thermal evolution of continental convergent belts. Journal of Geophysical Research 86 (B7), 6115–6132.

Houseman, G.A., Neil, E.A., Kohler, M.D., 2000. Lithospheric instability beneath the Transverse Ranges of California. Journal of Geophysical Research 105 (16), 237-216.

Jiménez-Munt, I., Negredo, A.M., 2003. Neotectonic modelling of the western part of the Africa–Eurasia plate boundary: from the Mid-Atlantic ridge to Algeria. Earth and Planetary Science Letters 205 (3), 257–271.

Jiménez-Munt, I., Fernández, M., Vergés, J., Afonso, J.C., García-Castellanos, D., Fullea, J., 2010. Lithospheric structure of the Gorringe Bank: insights into its origin and tectonic evolution. Tectonics 29 (5), TC5019.

Jiménez-Munt, I., Fernández, M., Vergés, J., Garcia-Castellanos, D., Fullea, J., Pérez-Gussinyé, M., Afonso, J.C., 2011. Decoupled crust–mantle accommodation of Africa–Eurasia convergence in the NW Moroccan margin. Journal of Geophysical Research 116 (B8), B08403.

Katz, R., Spiegelman, M., Langmuir, C., 2003. A new parameterization of hydrous mantle melting. Geochemistry, Geophysics, Geosystems 4 (9), 1073.

Lee, C., Lenardic, A., Cooper, C.M., Niu, F., Levander, A., 2005. The role of chemical boundary layers in regulating the thickness of continental and oceanic thermal boundary layers. Earth and Planetary Science Letters 230 (3–4), 379–395.

Lindquist, K.G., Engle, K., Stahlke, D., Price, E., 2004. Global topography and bathymetry grid improves research efforts. Eos, Transactions of the American Geophysical Union 85 (19), 186.

Lorinczi, P., Houseman, G.A., 2009. Lithospheric gravitational instability beneath the Southeast Carpathians. Tectonophysics 474 (1–2), 322–336.

Marotta, A.M., Fernández, M., Sabadini, R., 1998. Mantle unrooting in collisional settings. Tectonophysics 296 (1), 31–46.

Marotta, A.M., Fernández, M., Sabadini, R., 1999. The onset of extension during lithospheric shortening:a two-dimensional thermomechanical model for lithospheric unrooting. Geophysical Journal International 139 (1), 98–114.

Missenard, Y., Cadoux, A., 2012. Can Moroccan Atlas lithospheric thinning and volcanism be induced by Edge-Driven Convection? Terra Nova 24 (1), 27–33.

Missenard, Y., Zeyen, H., Frizon de Lamotte, D., Leturmy, P., Petit, C., Sébrier, M., Saddiqi, O., 2006. Crustal versus asthenospheric origin of relief of the Atlas Mountains of Morocco. Journal of Geophysical Research 111 (B3), B03401.

Missenard, Y., Saddiqi, O., Barbarand, J., Leturmy, P., Ruiz, G., Haimer, El, Frizon de Lamotte, D., 2008. Cenozoic denudation in the Marrakech High Atlas, Morocco: insight from apatite fission-track thermochronology. Terra Nova 20 (3), 221–228.

Molnar, P., Houseman, Gregory A., 2004. The effects of buoyant crust on the gravitational instability of thickened mantle lithosphere at zones of intracontinental convergence. Geophysical Journal International 158 (3), 1134–1150.

Moresi, L., Solomatov, V., 1998. Mantle convection with a brittle lithosphere: thoughts on the global tectonic styles of the Earth and Venus. Geophysical Journal International 133 (3), 669–682.

Moresi, L., Dufour, F., Mühlhaus, H., 2003. A Lagrangian integration point finite element method for large deformation modeling of viscoelastic geomaterials. Journal of Computational Physics 184 (2), 476–497.

Nikolaeva, K., Gerya, T.V., Marques, F.O., 2010. Subduction initiation at passive margins: numerical modeling. Journal of Geophysical Research 115 (B3), B03406.

Parsons, B., Sclater, J.G., 1977. An Analysis of the Variation of Ocean Floor Bathymatry and Heat Flow with Age. Journal of Geophysical Research 82 (5) (October 14).

Phipps Morgan, J., 1997. The generation of a compositional lithosphere by mid-ocean ridge melting and its effect on subsequent off-axis hotspot upwelling and melting. Earth and Planetary Science Letters 146 (1–2), 213–232.

Poudjom Djomani, Y.H., O'Reilly, S.Y., Griffin, W.L., Morgan, P., 2001. The density structure of subcontinental lithosphere through time. Earth and Planetary Science Letters 184 (3), 605–621.

Ribe, N., 2010. Bending mechanics and mode selection in free subduction: a thin-sheet analysis. Geophysical Journal International 180 (2), 559–576.

Ribe, N., Stutzmann, E., Ren, Y., van der Hilst, R.D., 2007. Buckling instabilities of subducted lithosphere beneath the transition zone. Earth and Planetary Science Letters 254 (1–2), 173–179.

Rosenbaum, G., Lister, G.S., Duboz, C., 2002. Relative motions of Africa, Iberia and Europe during Alpine orogeny. Tectonophysics 359 (1), 117–129.

Schellart, W.P., Stegman, D.R., Farrington, R., Moresi, L., 2011. Influence of lateral slab edge distance on plate velocity, trench velocity, and subduction partitioning. Journal of Geophysical Research 116 (B10), B10408.

Schubert, G., Turcotte, D.L., Olson, P., 2001. Mantle Convection in Earth and Planets 2001st ed. Cambridge Univ Press, UK.

Seber, D., Barazangi, M., Aissa Tadili, B., Ramdani, M., Ibenbrahim, A., Ben Sar, D., 1996. Three-dimensional upper mantle structure beneath the intraplate Atlas and interplate Rif mountains of Morocco. Journal of Geophysical Research 101 (B2), 3125.

Stegman, D.R., Farrington, R., Capitanio, F.A., Schellart, W., 2010. A regime diagram for subduction styles from 3-D numerical models of free subduction. Tectonophysics 483 (1–2), 29–45.

Stein, C.A., Stein, S., 1992. A model for the global variation in oceanic depth and heat flow with lithospheric age. Nature 359 (6391), 123–129.

Stern, R.J., 2004. Subduction initiation: spontaneous and induced. Earth and Planetary Science Letters 226 (3–4), 275–292.

Stixrude, L., Lithgow-Bertelloni, C., 2007. Influence of phase transformations on lateral heterogeneity and dynamics in Earth's mantle. Earth and Planetary Science Letters 263 (1–2), 45–55.

Teixell, A., Arboleya, M.L., Julivert, M., Charroud, M., 2003. Tectonic shortening and topography in the central High Atlas (Morocco). Tectonics 22 (5), 1051.

Teixell, A., Ayarza, P., Zeyen, H., Fernández, M., Arboleya, M.L., 2005. Effects of mantle upwelling in a compressional setting: the Atlas Mountains of Morocco. Terra Nova 17 (5), 456–461.

Torne, M., Fernández, M., Carbonell, J., Banda, E., 1995. Lithospheric transition from continental to oceanic in the west Iberia Atlantic margin. In: Banda, E., Torne, M., Talwani, M. (Eds.), NATO ASI Series. Springer, Netherlands, pp. 247–263.

Turcotte, D.L., Oxburgh, E.R., 1967. Finite amplitude convective cells and continental drift. Journal of Fluid Mechanics 28, 29–42.

Turcotte, D.L., Schubert, G., 1982. Geodynamics 450.

Valera, J.L., Negredo, A.M., Jiménez-Munt, I., 2011. Deep and near-surface consequences of root removal by asymmetric continental delamination. Tectonophysics 502 (1), 257–265.

Verges, J., Fernández, M., 2012. Tethys–Atlantic interaction along the Iberia–Africa Plate Boundary: the Betic–Rif Orogenic System. Tectonophysics 1–71.

VilÃ, M., Fernández, M., Jiménez-Munt, I., 2010. Radiogenic heat production variability of some common lithological groups and its significance to lithospheric thermal modeling. Tectonophysics 490 (3), 152–164.

Zeyen, H., Ayarza, P., Fernández, M., Rimi, A., 2005. Lithospheric structure under the western African–European plate boundary: a transect across the Atlas Mountains and the Gulf of Cadiz. Tectonics 24 (2) (pp.n/a–n/a).

Zitellini, N., Gràcia, E., Matias, L., Terrinha, P., Abreu, M.A., DeAlteriis, G., Henriet, J.P., Dañobeitia, J.J., Masson, D.G., Mulder, T., Ramella, R., Somoza, L., Diez, S., 2009. The quest for the Africa–Eurasia plate boundary west of the Strait of Gibraltar. Earth and Planetary Science Letters 280 (1–4), 13–50.

Zlotnik, S., Afonso, J.C., Díez, P., Fernández, M., 2008. Small-scale gravitational instabilities under the oceans: implications for the evolution of oceanic lithosphere and its expression in geophysical observables. Philosophical Magazine 88 (28–29), 3197–3217.